Tribology International 185 (2023) 108536

Contents lists available at ScienceDirect

Tribology International

journal homepage: www.elsevier.com/locate/triboint

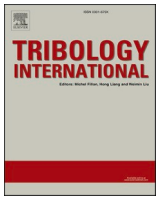

Tribo-oxidation of a brake friction couple under varying sliding conditions

Fabian Limmer *, Peter C. Brooks, Carl Gilkeson, Shahriar Kosarieh, David C. Barton

University of Leeds, School of Mechanical Engineering, Leeds, UK

ARTICLE INFO

Keywords:
Sliding friction
Dry friction
Brakes

ABSTRACT

This study explores a common parameter that is used to describe the energy input into a friction pairing in pin-on-disc investigations, the *pv*-value. The impacts of multiple sliding speed, *v*, and contact pressure, *p*, combinations were investigated while keeping their product, the *pv*-value at a constant level. The chosen tests for this study consisted of steady-state drag braking applications on a small-scale test bench. The actual contact area on the friction material's surface was measured after the tests and correlated to the steady-state temperature, *T*, that was reached during testing. The tribological interface showed sensitivity towards the different sliding and loading conditions including a shift in oxidising states of the iron contents of the friction couples. The sliding and loading conditions were reversed after the transition of oxidising states in order to investigate their impact. The results show that the oxidising states dynamically react to the operating conditions, but the overall frictional performance of the system can remain at an altered level due to enduring changes in the actual contact area and the thermal response of the friction couple with the transition in oxidising states.

1. Introduction

The driver of an automotive vehicle can reduce driving speed by pressing their foot on the brake pedal. This serves to dramatically increase brake line pressure which in turn presses brake pads against a disc that is rigidly connected to each wheel. Friction at the sliding interface between disc and pad causes the vehicle to slow down, depending on the applied pressure.

In today's vehicles which are still mainly powered by internal combustion engines, the friction brake is the main system used for deceleration, meaning that it is used quite frequently and with considerable power output. The automotive sector, however, is shifting its focus more towards electric vehicles in an effort to reduce global exhaust emissions. Projection shows that a global share of electric vehicle sales could reach 16% in 2025, rising as high as 90% for some larger markets by 2040 [1]. These particular vehicles have the advantage of recuperation, meaning that they can use the electric motors as generators to decelerate the vehicle; this also serves to harvest energy for charging the batteries. This, together with the prospect of autonomous vehicles will likely lead to reduced friction braking power requirements in the medium to longer term [2]. Consequently, the temperatures that are typically reached at the friction interface could be significantly lower. One of the challenges of this is that reduced brake disc temperatures can result in a higher corrosion risk, depending on the friction couple employed [3].

An issue with studying the effects of future load profiles through vehicle testing or full-size inertia dynamometer testing is that they are extremely time-consuming and costly. To circumvent these issues, first screenings are often carried out on smaller-scale tribometers. Two of the dominant parameters that are adjustable on most tribometers are: (i) the nominal contact pressure, *p*, between the brake disc and pad and (ii) the sliding speed, *v*. These two parameters are often represented as a product, the so-called *pv*-value. Past research has reported *pv*-values representing real braking conditions in the range of 0.3–24 MPa m/s [4-6]. A third important tribological parameter is the interface temperature, *T*, but this is highly variable and difficult to measure in a high friction contact such as a friction brake.

Research has also shown that the tribological processes taking place at the pad-disc sliding interface are very sensitive to the above-mentioned controllable *p-v* parameters. It is therefore reasonable to assume that the friction coefficient will change with varying sliding speed and normal load.

Eriksson et al. [7] observed the processes in the sliding interface using a glass brake disc and described the general contact situation as follows [8]. As the brake pad comes into contact with the brake disc (first bodies), debris is formed by the wear of the two bodies. More wear resistant constituents of the pad will start protruding forming first contact sites and carrying the load. These are also called the primary contact plateaux. The wear debris travels through the sliding interface

* Corresponding author.
E-mail address: mnfli@leeds.ac.uk (F. Limmer).

https://doi.org/10.1016/j.triboint.2023.108536
Received 22 November 2022; Received in revised form 16 March 2023; Accepted 18 April 2023
Available online 20 April 2023

(third body) until it ends up in front of a primary plateau where it is stopped. As more wear debris starts piling up in front of the primary plateau, it is compacted and agglomerates to a flat patch sometimes called the secondary plateau. These plateaux (primary and secondary) separate the two first bodies from another and carry the load as well as accommodate the velocity difference. Their size and distribution can vary with sliding speed, contact pressure, temperature and brake pad composition. The areas of real contact are even smaller than the contact plateaux as these are irregularly appearing small points of contact within the plateaux.

Rhee et al. [9] investigated different high-copper and copper-free friction material formulations sliding against a cast iron disc. The authors observed a generally decreasing friction coefficient for increasing nominal contact pressure over a broad range of sliding speeds although the friction coefficient sometimes also increased with increasing pressure under certain sliding speeds.

Wahlström et al. [6] performed steady-state drag braking tests on a small-scale tribometer using a low-metallic friction material and a cast iron rotor. Their results show a decreasing friction coefficient with increasing nominal contact pressure for slow sliding speeds (1 m/s) and the opposite behaviour at higher sliding speeds (3 m/s). The authors reasoned that below a threshold temperature (around 200 °C in this case) increasing the nominal contact pressure will increase the wear debris formation and create a thicker tribofilm (contact plateaux) which in turn will decrease the friction coefficient [10]. Above the threshold temperature, thermal degradation of the resin will cause a disruption of the tribofilm, increasing the friction coefficient. The same trend of decreasing friction coefficient was observed when increasing the sliding speed and this was also linked to an increase in the wear debris formation.

Ostermeyer et al. [11] conducted experiments on a purposefully designed tribometer using a full-scale disc together with scaled friction material specimens. For a series of braking applications lasting up to 10 s each, the authors also found a decrease in the friction coefficient with increasing speed as well as with increasing nominal contact pressure. The contact plateaux, however, were found to decrease with increasing speed and increase with increasing nominal contact pressure. The authors also observed a decrease in loose wear debris on the brake pad surface and identified a trend of increasing friction coefficient with an increased appearance of the loose wear debris areas. The authors concluded that there must be another load carrying patch other than the ones Eriksson et al. [7] identified and proposed the mechanism to be a self-locking of the particles.

Gramstat [12] investigated the dynamic situation of the contact plateaux on a global scale using a glass brake disc and found a generally decreasing brake torque with an increase in the contact plateaux size. The author also identified that the wear debris travelling through the interface can make a significant contribution to the contact area and found a general trend of increasing braking torque with an increase in the areas of wear debris travel. The effect of decreasing braking torque with increasing contact plateaux area could therefore be explained by Gramstat's observation that the increase in contact plateaux area actually reduced the total contact area.

One of the most important tribological processes that take place during braking, in the case that one or both counterparts contain iron, is an accelerated corrosion process more specifically called tribo-oxidation. This accelerated oxidation of iron is caused due to the heat generated by the friction force. Fig. 1 shows this oxidation cycle generalized for metals [13]. The heat from the friction process and oxygen from the surrounding air play a key role in the oxidation of iron which can form different kinds of oxides. It is more specifically the flash temperatures at the points of real contact that determine which oxidation state is reached. Iron oxidises in the form of haematite (α-Fe_2O_3) usually up to temperatures of 450 °C. The next highest oxidation state, magnetite (Fe_3O_4), forms predominantly at a temperature range between 450 °C and 600 °C. The very highest oxidation state, wüstite

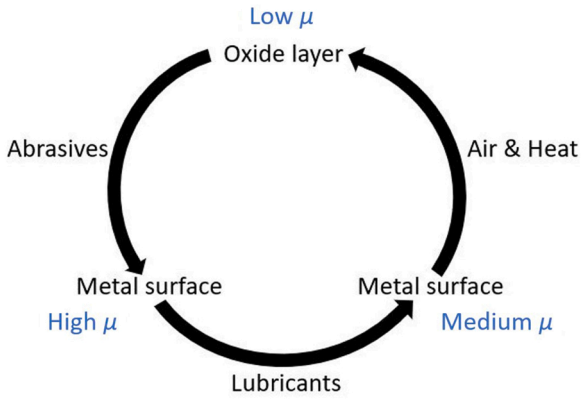

Fig. 1. Cycles of metals in friction materials.

(FeO), is formed at temperatures above 600 °C [14]. These transformations however are only observed if enough oxygen is in the surrounding environment.

In cases where the tribo-oxidation takes place under reduced oxygen conditions (often found in lubricated contacts), magnetite has been reported to form at temperatures as low as 150 °C [15]. Hinrichs et al. [16] subjected a full-scale brake system to moderate-to-high loading conditions (AK-Master) and reported magnetite to be the primary iron oxide formed during the braking process. Verma et al. [17] utilised a small-scale system under drag braking operation and moderate loading conditions; they found haematite to be the predominantly formed oxide. Alemani et al. [18] conducted tests, also using a small-scale system, including the collection and analysis of the airborne wear debris during testing. The authors found airborne wear debris consisting of haematite and elemental iron under light loading conditions and wear debris consisting of haematite and magnetite during higher loading conditions. Noh et al. [19] introduced iron and iron oxide particles to the sliding interface of a scaled dynamometer system. The authors found the highest friction oscillations when Fe_2O_3 particles were introduced and attributed this to the high static friction coefficient of this oxide. Davin et al. [20] investigated the effect of reduced oxygen in the atmosphere on the sliding conditions of a brake system using a small-scale setup. They found that, as the oxygen content in the atmosphere is reduced, the number of secondary contact plateaux (which largely consisted of iron oxide) reduces without changing their chemical content. The study, however, did not investigate the specific oxidation stage of the iron oxide.

Qi et al. [21] conducted experiments applying different thermocouple methods to record the temperatures during braking. Using an open hot junction thermocouple embedded into the friction material, the authors reported the temperature recorded by this thermocouple was 225 °C higher than that measured by a rubbing thermocouple located on the disc surface. The authors interpreted this temperature discrepancy to reflect the difference between the local contact temperature and the global disc temperature (background temperature).

The work presented in this paper focuses on investigating the reaction of a brake friction couple (including the friction, wear and contact characteristics) to a broad variation of contact pressure and sliding speed. From the known literature, most previous studies which have investigated the effects of varying these parameters have changed either or both parameters but have not kept their product, the pv-value, constant. Since for constant pad geometry and coefficient of friction, the pv-value is a measure of the rate of energy input (or power) of the tribosystem, testing at constant pv-value will be an additional consideration in this work.

2. Material and methods

The tests for this study were carried out on a benchtop tribometer (Bruker Universal Mechanical Tester TriboLab) with a pin-on-disc type setup (Fig. 2). The samples consisted of a commercial copper-free low-metallic friction material with the plan dimensions 30×10 mm and 10 mm initial thickness. The brake disc was made from grey cast iron (EN GJL 250) and has a diameter of 100 mm and a solid thickness of 10 mm. The surface of the disc was prepared using 320 grit sandpaper before testing to remove any larger machining marks [22]. The normal and friction forces were measured simultaneously with a single force sensor (Bruker DFH-50 G 500 N ± 0.005 N). The friction coefficient was directly calculated from the two force output signals. The temperature of the brake disc was measured on the disc surface immediately adjacent to the friction track using a rubbing thermocouple (TC Brake Disc Rubbing Thermocouple 850 °C ± 2.5 °C). The temperature of the friction material samples was measured using an embedded thermocouple (TC Embedded Brake Pad Thermocouple 250 °C ± 2.5 °C).

A constant pv-value of 0.76 MPa m/s was chosen to simulate mild sliding conditions [23]. Starting from the lowest speed-highest pressure combination, the speed was then doubled, and the load was halved for each of the following three tests. The controlled parameters for each test condition are listed in Table 1. The range of sliding speeds at the brake friction interface was 1.31–10.45 m/s which corresponds to vehicle speeds of about 12–100 km/h, covering the typical range of everyday driving speeds. The range of nominal contact pressures at the brake friction interface was 0.58–0.07 MPa which corresponds to brake line pressures of about 1.4–11.8 bar, covering the range from pressures observed in electric vehicles up to those seen under mild braking in conventional vehicles [3]. Each test had a duration of 120 min which was sufficient for the system to reach steady-state conditions. Furthermore, enough time was given for the system to cool back down to room temperature in between each test. The friction couple was subjected to a running-in application at a nominal contact pressure of 0.05 MPa and a sliding speed of 5.5 m/s (0.275 MPa m/s) for 30 min before the first test.

Table 1
Range of operating conditions for the tests.

Test Condition	Sliding Speed (m/s)	Normal Load (N)	Nominal Contact Pressure (MPa)
1	1.31	174	0.58
2	2.62	87	0.29
3	5.24	45	0.15
4	10.47	21	0.07

After each test, the friction material samples were analysed using an optical measuring system (Bruker Alikona InfiniteFocus) to capture the contact plateaux on the friction material surfaces based on the image segmentation method that was introduced by Neis et al. [24]. The method is based on the principle that the protruding contact plateaux present a smoother, flatter surface than the surrounding lowlands [25] so they can be detected using light microscopy [26]. Fig. 3 shows an example of how the plateaux area is obtained. The top image visually displays a friction material's surface after testing using ring light illumination. The middle image shows the contact plateaux under high contrast to the lowlands using coaxial illumination and the bottom image shows the segmented surface which is used for obtaining the contact area. Single images were taken using an objective with 5x magnification, then image stitching was performed before segmentation. This ensured that the surface characterisation captured the entire friction material area. Chemical information of the friction material surfaces was obtained using Raman spectroscopy (Renishaw inVia). The mass loss of the friction material samples, and brake disc was measured using analytical balances (Mettler Toledo XP 205 with a resolution of 10 μg for the friction material and My Weigh iBalance iM01 with a resolution of 0.01 g for the brake disc). An overview of the conducted tests is given in Table 2.

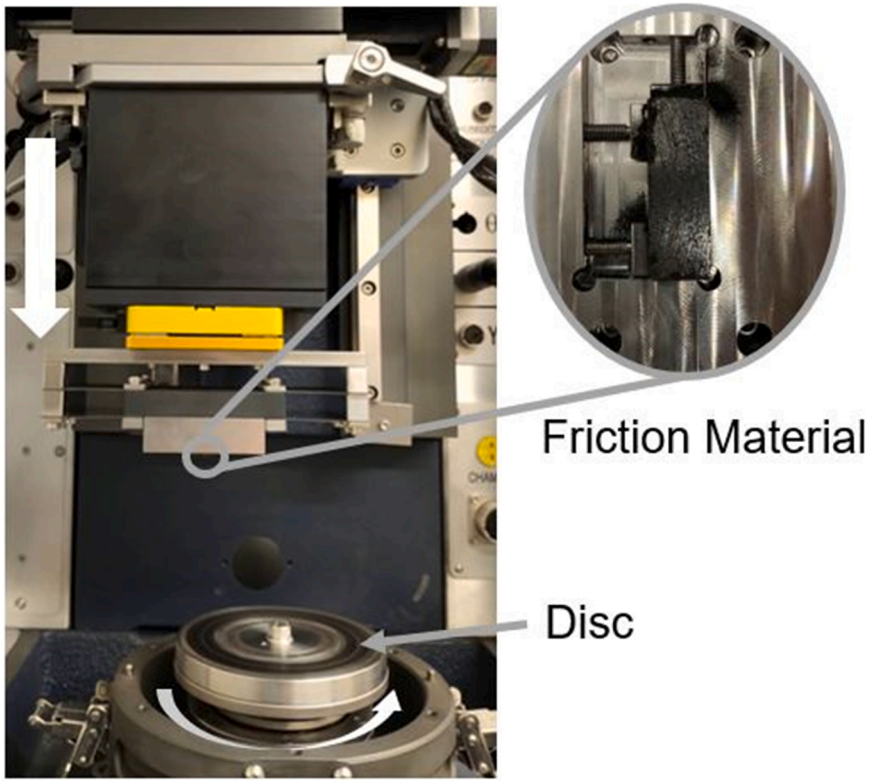

Fig. 2. Experimental Setup.

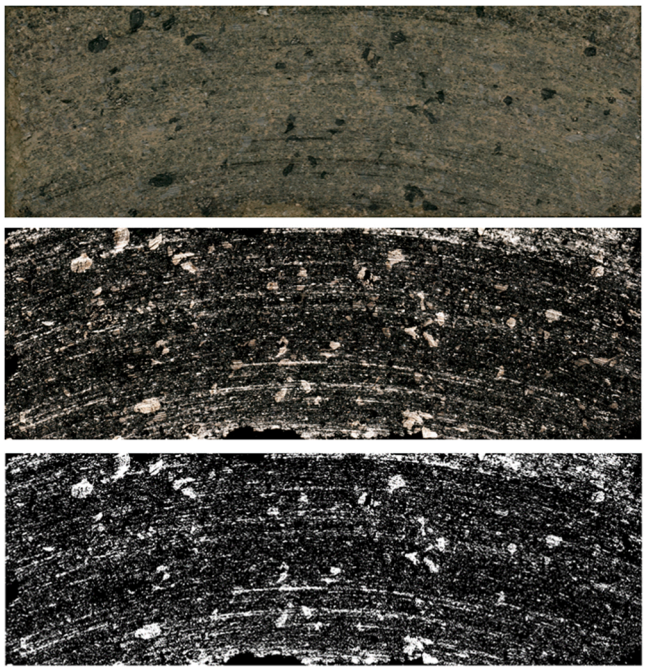

Fig. 3. Example of image segmentation method showing a friction material's surface under ring light illumination (top), coaxial illumination (middle) and after segmentation.

Table 2
Summary of all conducted tests.

Test	Comments
1.1 – 4.1	After conducting the run-in procedure, succession through all test conditions 1–4 using same friction material and brake disc surface
4.2 – 3.2	Execution of test condition 4 then 3 (reversed order) using same friction material and brake disc surface
3.3 – 3.5	Repeat execution of test condition 3 using same friction material and brake disc surface
3.6 – 3.8	Repeated execution of test condition 3 using virgin friction material and resurfaced brake disc to include measurement of wear and pad temperature following run-in procedure
4.3 – 4.5	Repeated execution of test condition 4 using virgin friction material and resurfaced brake disc to include measurement of wear and pad temperature following run-in procedure
3.9 – 4.6	Execution of test conditions 3 then 4 with 2 h cool-down in-between using virgin friction material and resurfaced brake disc to include disc temperature measurement on the rubbing track following run-in procedure

3. Results

Fig. 4a shows the evolution of the friction coefficient for the initial series of tests (designated tests 1.1–4.1). From test 1.1 (highest load and lowest sliding speed) to test 3.1, there is a noticeable trend of decreasing friction coefficient (0.56–0.47) once steady-state conditions have been reached. Test 4.1 (lowest load and highest sliding speed) however shows an irregular behaviour with the friction coefficient for test 4.1 being, on average, the highest for all tests (0.62). The mean friction coefficients (Mean COF) of the steady-state region of each test are listed in Table 3. Since the disc temperature takes longer to settle to a steady state than the friction coefficient, the mean disc temperature was calculated from 6000 s onwards until the end of the test.

The disc temperature development is shown in Fig. 4b. As with the friction coefficient, there was a decreasing trend from test 1.1–3.1 with the temperature reaching 217 °C for test 1.1 compared with 159 °C for test 3.1. The highest friction recorded for test 4.1 however, did not result in a correspondingly high disc temperature and in fact, the temperature (162 °C) for this low pressure, high speed test reached a value close to test 3.1.(159 °C).

Measuring the contact plateaux on the friction materials surface after each test revealed a trend of increasing predicted plateaux areas from test 1.1 to test 3.1, as shown in Table 3. The average friction power was calculated from the steady-state regions of each test by multiplying the friction force with the sliding speed (at the mean friction radius). Plotting the average friction power against the contact area (Fig. 5) shows a decrease of 20.75 W with an increase in the plateaux area of 18.2% for tests 1.1–3.1. However, the highest friction power was reached during test 4.1 with an average of 140 W, an increase of over 33 W, while the plateaux area had actually decreased by 5.7% from that measured for test 3.1.

Fig. 6 shows the surface of the friction material captured with a digital camera after test 3.1 (Fig. 6a) and test 4.1 (Fig. 6b). Up to test 3.1, the friction material surface looks typical for a low-metallic friction material after operation by virtue of it being dark in colour. In contrast, the friction material surface appears very reddish after test 4.1. Raman investigations of the spectrum (Fig. 7) show that for the friction material surface used in test 3.1 (Fig. 7a), the peak intensity of magnetite (Fe_3O_4) occurs at 680 cm^{-1} with two disordered graphite (C) peaks seen at 1366 cm^{-1} and 1596 cm^{-1}; this is consistent with the findings from [27]. The friction material surface from test 4.1 (Fig. 7b) shows a different spectrum. Peaks at 229 cm^{-1}, 289 cm^{-1}, 407 cm^{-1} as well as the very broad peak at 1318 cm^{-1} are typical for haematite (Fe_2O_3) [28].

Test conditions 3 and 4 were then repeated in reverse order (designated tests 3.2 and 4.2 respectively) meaning that test condition 4 was carried out before test condition 3 this time to investigate whether the previously observed oxidation states and the friction coefficients would alter. Fig. 8 shows that the friction coefficient (Fig. 8a) for test 4.2 settled to around 0.6 as it did in the previous test whereas test 3.2 showed a different behaviour than before with the friction coefficient remaining at 0.6 as for test 4.2. The disc temperatures in Fig. 8b show that test 4.2 again settled at around 160 °C as in the previous test but test 3.2 this time settled at around 195 °C (36 °C higher than before).

Test condition 3 was then repeated three times to see if this change in the friction coefficient was consistent. Fig. 9 shows that for the three repeats, designated tests 3.3, 3.4 and 3.5 respectively, the friction coefficient remained at a near identical level. Table 4 again lists the mean of the coefficients of friction, as well as the mean disc temperature for this new set of repeat tests. The disc temperatures of test 3.2 and all repeats settled within ± 4 °C of 198 °C, demonstrating their consistency between tests.

To obtain further information about the wearing conditions and the division of the frictional heat between the two parts of the friction couple, two new friction material samples were prepared by drilling holes into the back side to accommodate a thermocouple. Both samples were subjected to the standard running-in application before performing three cycles of either test condition 3 or 4 respectively. The three cycles were run successively to generate measurable wear, with the friction material and disc being weighed before and after the three test cycles. Fig. 10 shows the friction coefficient (Fig. 10a), disc temperature and pad temperature (Fig. 10b) of the three further repeat cycles of test 3 (designated 3.6, 3.7 and 3.8). The mean friction coefficient was again around 0.6 and the measured disc temperature was 191 °C. The pad temperature reaches a steady state at 135 °C, approximately 56 °C lower than that of the disc. The results of the test 4 repeats (designated 4.3, 4.4 and 4.5) are shown in Fig. 11. The friction coefficient average was 0.65, the brake disc temperature was 171 °C and the pad temperature was 137 °C resulting in a disc-pad temperature difference of 34 °C. The pad temperatures for both test conditions 3 and 4 remained at a near identical level, showing only a difference of 2 °C while the average disc temperature for the three repeat cycles of test condition 3 was 20 °C higher than for the repeat cycles of test condition 4.

The mass loss accumulated over the three repeat cycles of test

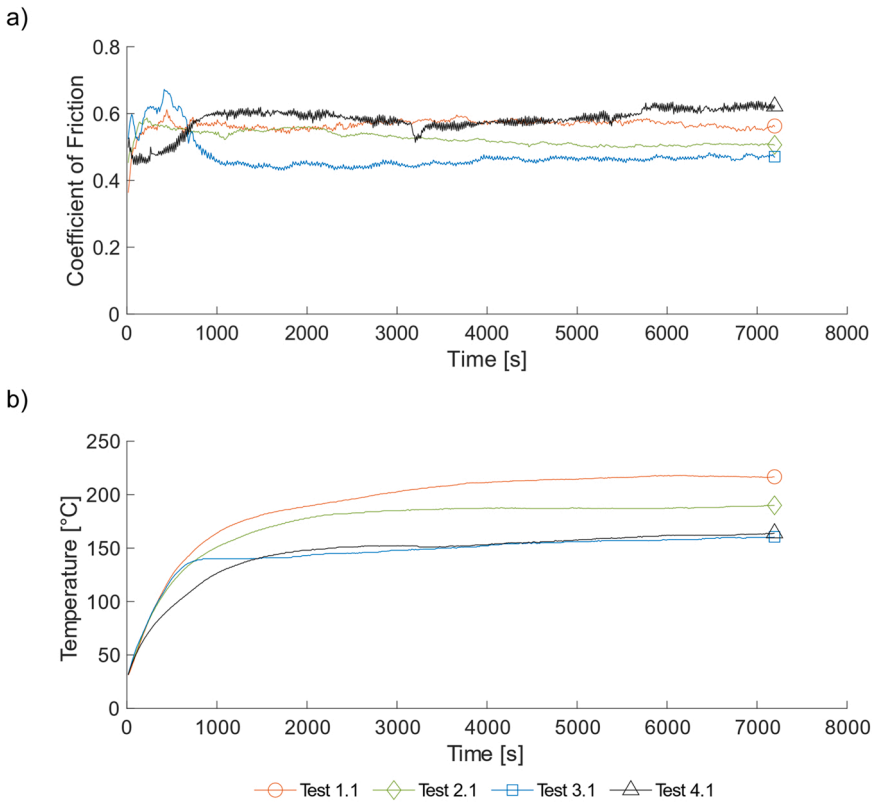

Fig. 4. a) friction coefficient and b) disc temperature evolution for tests 1.1–4.1.

Table 3
Results for tests 1.1 – 4.1.

Test No. (MPa, m/s)	Mean COF	Mean Disc Temp (°C)	Contact Area (%)
1.1 (p = 0.58, v=1.31)	0.56	217	19.3
2.1 (p = 0.29, v=2.62)	0.51	188	28.2
3.1 (p = 0.15, v=5.24)	0.47	159	37.5
4.1 (p = 0.07, v=10.47)	0.62	162	31.8

conditions 3 and 4 is displayed in Fig. 12. For test condition 3 (tests 3.6, 3.7 and 3.8), where magnetite is the dominantly formed oxide, all the friction couples total mass loss (0.158 g) came from the pad (0.178 g), with the brake disc actually gaining mass (−0.02 g) throughout the tests, indicating a material transfer occurred from the pad to the disc. For test condition 4 (tests 4.3, 4.4 and 4.5), where the dominantly formed oxide is haematite, the friction couples mass loss (0.217 g) originates predominantly from the disc (0.14 g), with the pad contributing only 35% to the total mass loss (0.077 g).

The accumulated mass loss was related to the accumulated friction work in order to obtain a measure, also known as the Energy Wear Coefficient (EWC) [29], that more closely describes the friction couple's wear resistance under the given loading conditions. The EWC is generally defined as, $\alpha_v = V/(\sum E_d - \sum E_{dth})$ with V being the wear volume, E_d being the dissipated energy and E_{dth} being the threshold energy which is required for the initial transformation of the body's surface before wear generation begins. The wear, in this case, was measured as mass loss, M, and the threshold energy was assumed to be negligible. The EWC is therefore defined as, $\alpha_M = M/\sum E_d$.The EWC results, also shown in Fig. 12, indicate a 27% increase in EWC for the three repeat cycles of test condition 4 compared with the same cycles of test condition 3 meaning that the wear mass per unit work done by the friction couple is higher under these low pressure, high speed sliding conditions.

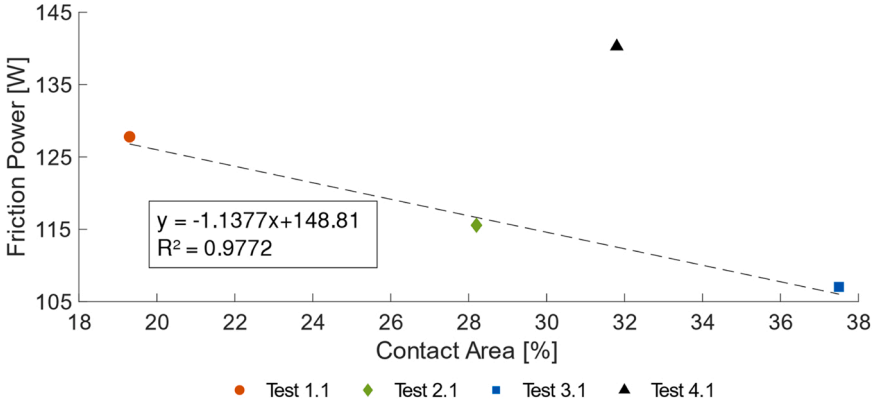

Fig. 5. Average friction power vs. contact area.

Fig. 6. Friction material surfaces after a) test 3 and b) test 4.

To obtain further information on the thermal effects of the transfer layer and the cooling characteristics of the brake disc under the test conditions 3 and 4, two rubbing thermocouples were placed on the brake disc surface. One was on the same position (next to the rubbing track) as in the previous tests and the other one was placed on the rubbing track behind the friction couple. A new friction material and a freshly surfaced brake disc were subjected to the running-in procedure followed by repeats of test condition 3 (designated test 3.9) and then test condition 4 (designated test 4.6). The test cycles were adjusted by adding a two-hour cooling period where the brake disc remains spinning at the same speed as during the braking event, but the pad is lifted away from the disc. Fig. 13 shows the friction coefficient as well as the on- and off-track temperature of the brake disc. For test 3.9, the mean coefficient of friction was 0.524, the on-track temperature reached 191 °C and the off-track temperature was 167 °C. A friction coefficient of 0.646 was reached during test 4.6 accompanied by a visible change in oxidising states. The temperatures reached 189 °C on the rubbing track and 164 °C next to the rubbing track. Both the on-track and off-track temperatures of tests 3.9 and 4.6 are, therefore, within 3 °C of each other with a temperature difference of around 25 °C between the on- and off-track temperatures. Both the on- and off-track temperatures level off to 42 °C ± 2 °C at the end of the 2-hour cooling period.

Cooling curves were calculated for the disc in the conventional way using the rubbing track temperature recording over the first 1000 s after the pad was lifted from the disc (Fig. 14). Based on Newton's law of cooling ($T_t - T_0 = (T_{t1} - T_0)e^{(-bt)}$), the cooling curves can be displayed through $\ln((T_t - T_0)/(T_{t1} - T_0)) = -bt$ [30] where T_t is the temperature at time t, T_{t1} is the temperature at the time when the pad is retracted from the disc and T_0 is the temperature of the surrounding air. The cooling coefficient, b, is given by the slope of the cooling curve which for both tests was a straight line as expected [31–33]. The cooling coefficient equalled to 0.0008 s^{-1} for test 3.9 and 0.0011 s^{-1} for test 4.6. The heat transfer coefficient, h, can be calculated from the cooling coefficient, b, using $h = bmC_P/A_S$ where m is the disc mass in kg, C_P is the specific heat capacity of cast iron (460 J/kgK) and A_S is the brake disc's surface area exposed to the surrounding environment (0.008943 m^2). The heat transfer coefficient calculated by this equation was 16 W/m^2K for test 3.9 and 22.63 W/m^2K for test 4.6. The cooling power of the disc, $\dot{Q}$, can be estimated using $\dot{Q} = hA_S(T_t - T_0)$. At the end of the 2 h cycle, the cooling capacity was estimated to be 19 W for test 3.9 and 26 W for test 4.6.

4. Discussion

The friction couple reacted with a decreasing friction coefficient during the progression through lighter loading conditions and increasing sliding speeds for the first 3 test conditions (test conditions 1–3). The increase in the contact plateaux area alongside the decrease in friction coefficient suggests that the total contact area is actually reduced by the growth of the contact plateaux as Gramstat [12] suggested. It is commonly observed that increasing either the sliding speed or the nominal contact pressure leads to a decrease in the coefficient of friction while the area of contact plateaux increases. The results suggest that when both parameters are changed simultaneously, increasing the sliding speed in this range of pv has a greater impact on generating more contact plateaux area than the reduction of the nominal contact pressure has on reducing it.

Further increase of the sliding speed and reduction of the nominal contact pressure (test condition 4) led to a shift in oxidising states that caused a significant change in the friction couple's behaviour. Although the total contact plateaux area is only slightly decreased, the coefficient

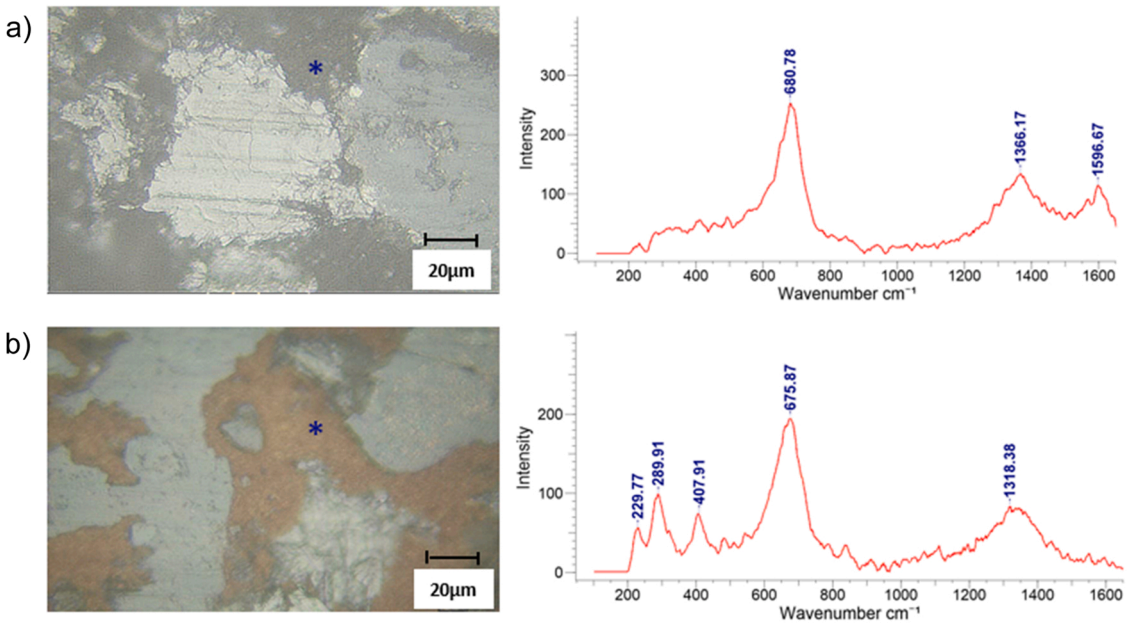

Fig. 7. Raman spectrum of the friction material surfaces after a) test 3 and b) test 4.

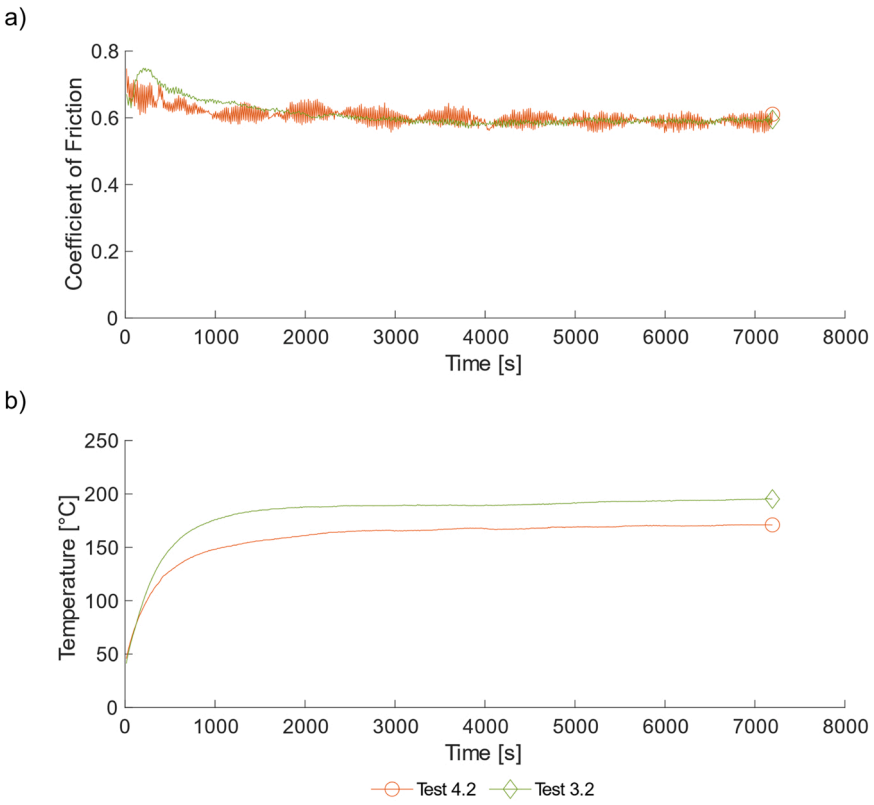

Fig. 8. a) friction coefficient and b) disc temperature evolution for test 3.2 and 4.2.

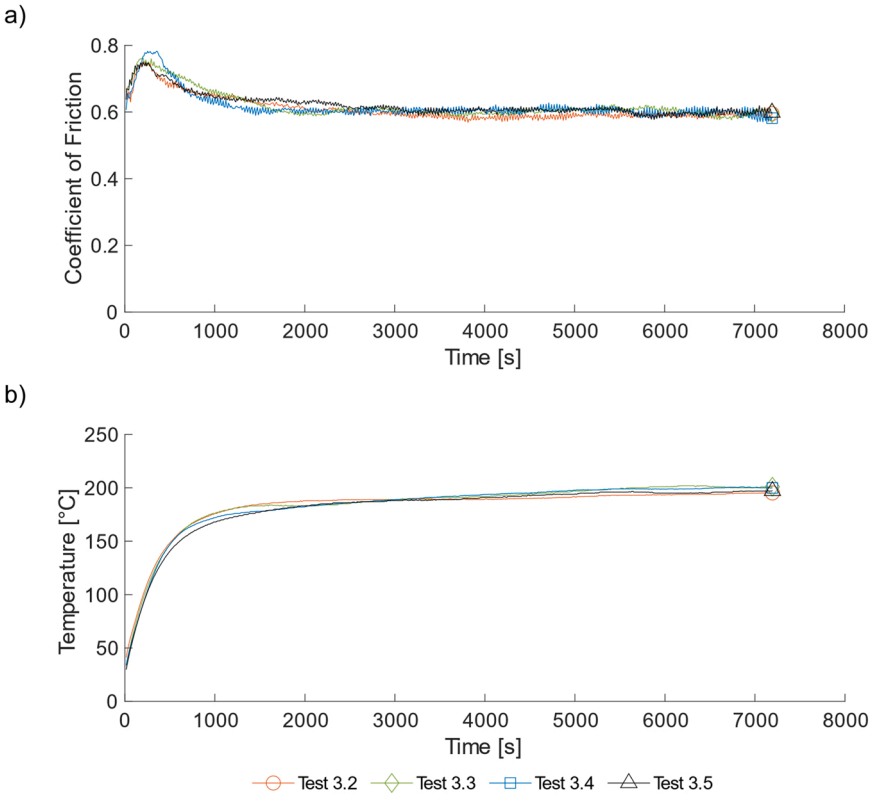

Fig. 9. a) friction coefficient and b) disc temperature evolution for test 3.2, 3.3, 3.4 and 3.5.

Table 4
Mean value of the friction coefficient for repeat tests 3.2 – 3.5.

Test No. (MPa, m/s)	Mean COF	Mean Disc Temp (°C)
3.2 ($p = 0.15$, v=5.24)	0.59	194
3.3 ($p = 0.15$, v=5.24)	0.59	201
3.4 ($p = 0.15$, v=5.24)	0.60	200
3.5 ($p = 0.15$, v=5.24)	0.60	196

of friction increased to a higher state than in test condition 1 but there was no increase in the disc temperature. The reason for the increase in friction could be due to the more abrasive nature of haematite [14]. The visible shift in oxidising states from magnetite to haematite indicated that the flash temperatures have dropped below the reported transition temperature of 450 °C. The question now is, if the brake disc's temperature doesn't rise with the increased friction power, where does the excess energy go? It is known that the sliding speed plays a significant role in the division of heat between the two bodies [34,35]. As the rotating speed is doubled from test to test and the nominal contact pressure is halved, the change of the sliding speed in terms of its numerical value is greatest from test condition 3–4. In general, the faster the rotating part of a friction couple moves, the less time there is for the temperature distribution to be established on the moving surface [36]. For the specific case of a brake system, however, there is another effect that takes place as the surface of the moving body (the brake disc) is under periodically reoccurring contact. At a higher rotational speed, the heat drag (peak disc surface temperature reached inside the friction interface) expands over a longer distance from the trailing edge of the pad until ultimately expanding all the way towards the leading edge of the friction interface. This more uniform thermal distribution in the body of the disc at high rotational speeds could favour the division of heat towards the disc because a greater mass of the disc is being heated to the measured maximum temperature [37,38]. In addition, since the true contact areas on the friction material's surface for test conditions 3 and 4 were not far apart (37.5% and 31.8% respectively), the fact that the thermal conductivity of haematite is approximately double that of magnetite over this temperature range [39], could mean that the haematite-containing third body layer will be a less effective thermal barrier for test condition 4. However, tests 3.9 and 4.6 (recall Fig. 13) demonstrate that both the actual disc temperatures as well as the on-track, off-track temperature differences are almost identical for both tests. This, together with the results from tests 3.6–3.8 and 4.3–3.5 (recall Fig. 12) indicating no significant change in the pad's temperatures with the change in oxidising states, suggests that there is no change in the division of heat with the change in oxidising states. Any such change in the heat partitioning would result in an increase in the pad material's temperature alongside the measured increase in friction power.

The increase in the rotational speed of the disc also impacts its cooling rate, mainly by means of increased convection with the environment. The increase in convective cooling with the increase in the disc's rotating speed accounts for an increase in cooling power of roughly 7 W (comparing results for tests 3.9 and 4.6). However, the increase in power input through the higher friction of test 4.6 approximates to 28 W, meaning that the observed phenomenon of largely unchanged temperatures with an increase in friction power cannot be explained simply by an increase in the cooling power of the disc. It is therefore reasonable to assume that the iron oxidation process itself could be the cause of this discrepancy between friction power and temperature rise, but more work needs to be done to confirm this.

The wear results show that the friction material is the only contributor to the friction couple's mass loss under the sliding conditions where magnetite is the main oxide produced (test condition 3). This indicates that the magnetite provides a good protection for the disc against wear with a material transfer taking place from the pad onto the disc. The drastic increase in the disc's mass loss when the main oxide formed

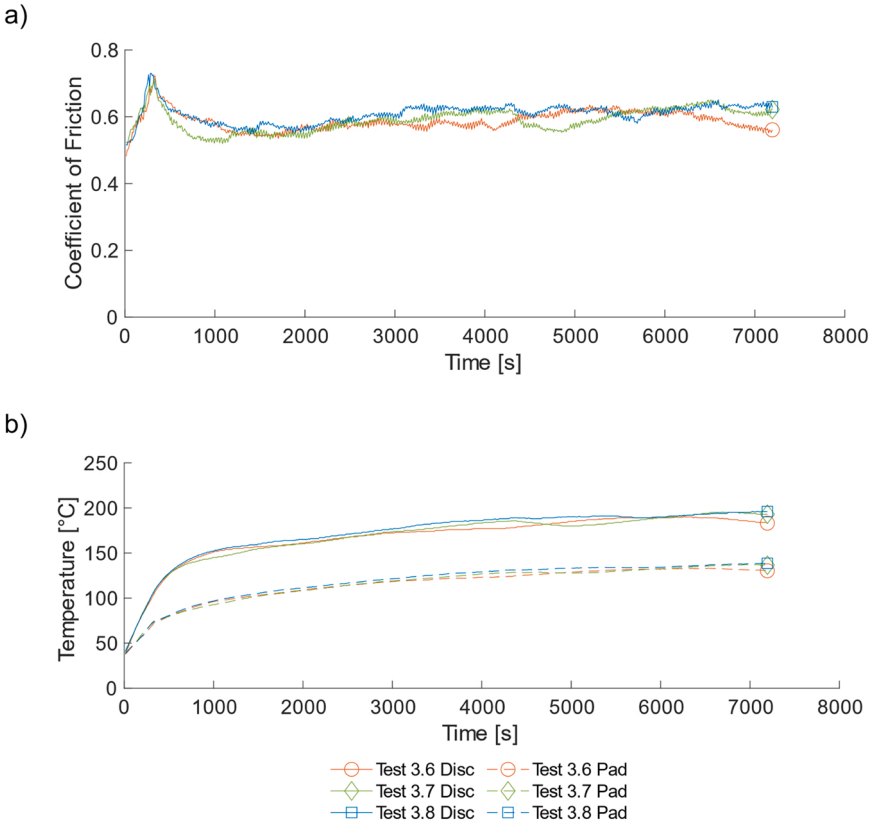

Fig. 10. a) friction coefficient, b) disc temperature and pad temperature evolution for test 3.6, 3.7 and 3.8.

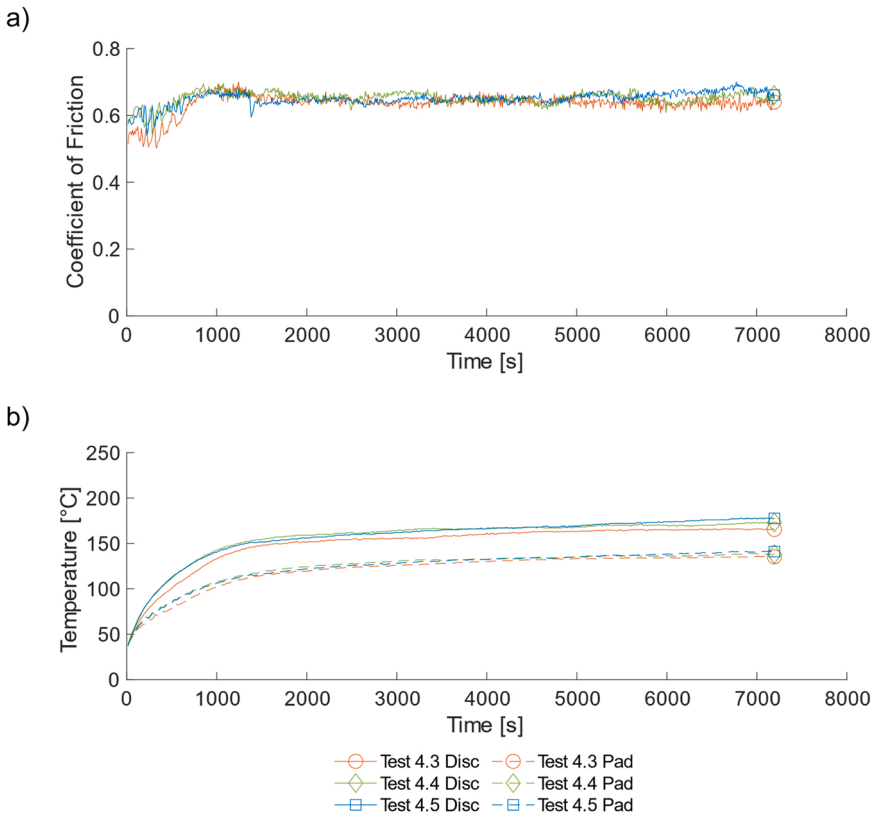

Fig. 11. a) Friction coefficient, b) disc temperature and pad temperature evolution for test 4.3, 4.4 and 4.5.

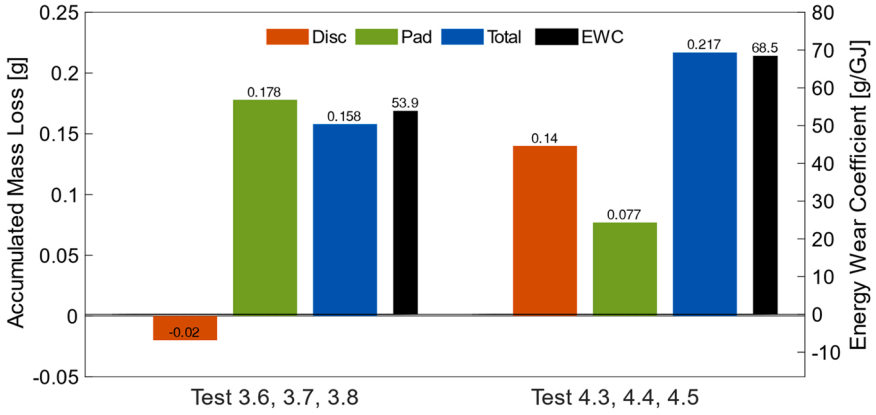

Fig. 12. Accumulated and normalised mass loss for tests 3.6, 3.7, 3.8 and 4.3, 4.4, 4.5.

changes to haematite suggests that this oxide does not allow the formation of a protecting surface layer for the disc which may be due to the more abrasive nature of haematite. The finding that the contact area also decreases slightly with the transition of the oxide states is another indicator for this more abrasive role. This obviously as implications for the amount, as well as the type, of wear debris emitted into the environment under these high speed, low pressure sliding conditions which may be typical for electric vehicles fitted with regenerative braking.

5. Conclusion

This study subjected a brake friction couple to different loading conditions through varying the sliding speed and contact pressure over a broad range while keeping their product, the pv-value, constant. The findings indicate that tribo-oxidation of an iron-containing brake system can produce different oxides under specific light loading conditions even with the same pv-value. Evaluating braking scenarios through their pv-values alone should therefore be done with caution because both parameters can have independent effects on the contact conditions; in this study, the iron oxidising states dramatically impacted the interface friction and temperature under identical pv-values. The unfavourable oxidising state (Fe_2O_3) has been found to appear at disc surface temperatures as high as 189 °C and the oxidising states have been shown to switch rapidly with a relatively small change in sliding conditions.

Some recommendations that can be drawn from this study are to adjust the friction material formulations in such a way that fewer and smaller contact plateaux are formed, specifically at higher sliding speeds, in order to promote high flash temperatures at lower braking pressures. Another approach could be through the sizing of brake systems, especially the brake disc for electric vehicles, to avoid any

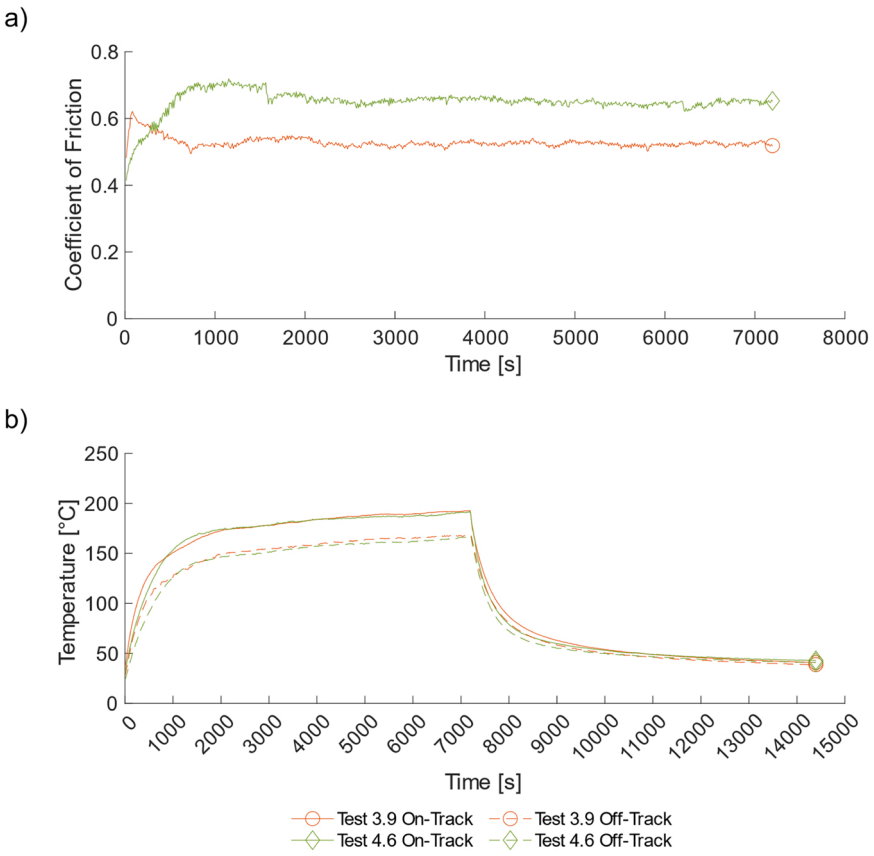

Fig. 13. a) Friction coefficient, b) rubbing track and disc temperature evolution for test 3.9 and 4.6.

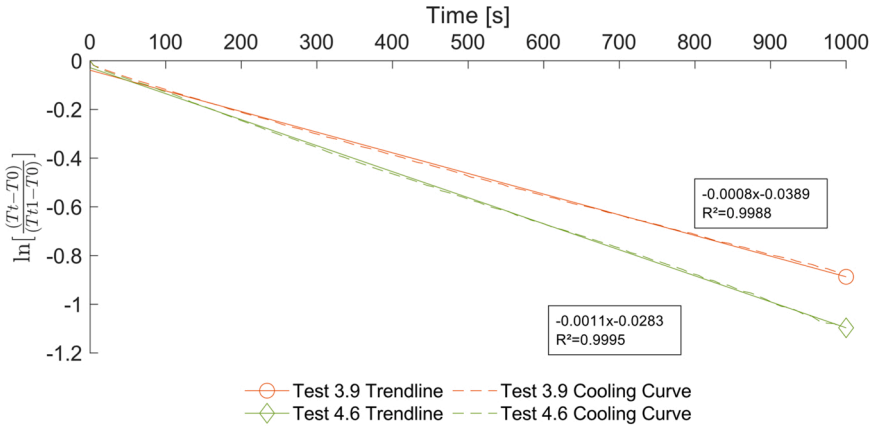

Fig. 14. Cooling curves from the rubbing track temperature of test 3.9 and test 4.6.

combinations of p, v and T scenarios where tribologically-accelerated formation of haematite could take place.

Since this study was carried out with small-scaled samples, these conclusions are only valid on a material level. Similar tests should be carried out on a full-scale disc brake dynamometer to investigate if these findings are also relevant on a brake system level. Further investigations with non-iron based friction couples would give more detailed insights and possibly reinforce the conclusion that the lower than expected brake disc surface temperatures under low pressure higher sliding speed conditions are caused by the transition in the oxidation process. The particulate emissions from both cast iron and non-iron friction couples under the different pv sliding conditions are also worthy of investigation. Such studies are possible with a modified form of the Leeds small-scale brake tribometer described in Limmer et al. [40].

Declaration of Competing Interest

The authors declare that they have no known competing financial interests or personal relationships that could have appeared to influence the work reported in this paper.

Data availability

The data that has been used is confidential.

Acknowledgements

This work has been funded by the Engineering and Physical Sciences Research Council, UK (EPSRC) Grant no.: EPL01629×1 and TMD

Friction Holdings GmbH, Germany. The authors also want to thank Emeritus Professor Tom Childs for the valuable discussions about the research which have led to the generation of new ideas.

References

[1] Bloomberg New Energy Finance: Electric Vehicle Outlook 2021 Executive Summary. Available online: https://bnef.turtl.co/story/evo-2021/page/1?teaser=yes.

[2] Meachair DÓ. Brake Robot, 2019. Available online: https://brakebetter.com/brake-robot/.

[3] Bode K, Tiedemann M. Wheel brakes for electric vehicles potentials and challenges. ATZ World 2017. https://doi.org/10.1007/s38311-017-0043-y.

[4] Briscoe BJ, Tweedale PJ. Aramid fiber friction - asbestos replacement in high friction materials. Inst Phys Conf Ser 1990.

[5] Straffelini G, Maines L. The relationship between wear of semimetallic friction materials and pearlitic cast iron in dry sliding. Wear 2013. https://doi.org/10.1016/j.wear.2013.08.020.

[6] Wahlström J, Matejka V, Lyu Y, Söderberg A. Contact Pressure and Sliding Velocity Maps of the Friction, Wear and Emission from a Low-Metallic/Cast-Iron Disc Brake Contact Pair. Tribol Ind 2017;39:460–70. https://doi.org/10.24874/ti.2017.39.04.05.

[7] Eriksson M, Lord J, Jacobson S. Wear and contact conditions of brake pads: Dynamical in situ studies of pads on glass. Wear 2001;249:272–8. https://doi.org/10.1016/S0043-1648(01)00573-7.

[8] Eriksson M, Bergman F, Jacobson S. On the nature of tribological contact in automotive brakes. Wear 2002;252:26–36. https://doi.org/10.1016/S0043-1648(01)00849-3.

[9] Rhee SK, Sriwiboon M, Tiempan N, Kaewlob K. The Normal-Load and Sliding-Speed Dependence of the Coefficient of Friction, and Wear Particle Generation Contributing to Friction: High-Copper and Copper-Free Formulations. SAE Tech Pap 2019. https://doi.org/10.4271/2019-01-2131. 2019-01-2131.

[10] Österle W, Dmitriev AI. Functionality of conventional brake friction materials - Perceptions from findings observed at different length scales. Wear 2011;271:2198–207. https://doi.org/10.1016/j.wear.2010.11.035.

[11] Ostermeyer GP, Wilkening L. Experimental Investigations of the Topography Dynamics in Brake Pads. SAE Int J Passeng Cars - Mech Syst 2013;6:1398–407. https://doi.org/10.4271/2013-01-2027.

[12] Gramstat S. Methoden der in-situ Visualisierung der Reibzonendynamik trockenlaufender Reibpaarungen unter Ergänzung physikalischer und chemischer Charakterisierungen der Reibpartner. Kraftfahrzeugtechnische Berichte. 7. University of Ilmenau; 2014.

[13] Dante R.C. Handbook of Friction Materials and their Applications. Woodhead Publishing Limited; 2016. https://doi.org/10.1192/bjp.111.479.1009-a.

[14] Quinn TFJ. Review of oxidational wear. Part I: Orig Oxid wear Tribol Int 1983;16:257–71. https://doi.org/10.1016/0301-679X(83)90086-5.

[15] Schöfer J. Tribologische Initialprozesse bei Selbstpaarungen aus dem Stahl 100Cr6 unter reversierender Gleitbeanspruchung in einem kraftstoffähnlichen Isoparaffingemisch. University of Karlsruhe, 2001.

[16] Hinrichs R, Vasconcellos MAZ, Österle W, Prietzel C. A TEM snapshot of magnetite formation in brakes: The role of the disc's cast iron graphite lamellae in third body formation. Wear 2011. https://doi.org/10.1016/j.wear.2010.11.008.

[17] Chandra Verma P, Menapace L, Bonfanti A, Ciudin R, Gialanella S, Straffelini G. Braking pad-disc system: Wear mechanisms and formation of wear fragments. Wear 2015;322–323:251–8. https://doi.org/10.1016/j.wear.2014.11.019.

[18] Alemani M, Gialanella S, Straffelini G, Ciudin R, Olofsson U, Perricone G. Dry sliding of a low steel friction material against cast iron at different loads: Characterization of the friction layer and wear debris. Wear 2017;376–377:1450–9. https://doi.org/10.1016/j.wear.2017.01.040.

[19] Noh HJ, Jang H. Friction instability induced by iron and iron oxides on friction material surface. Wear 2018;400–401:93–9. https://doi.org/10.1016/j.wear.2017.12.025.

[20] Davin E, Cristol AL, Brunel JF, Desplanques Y. Wear mechanisms alteration at braking interface through atmosphere modification. Wear 2019;426–427:1094–101. https://doi.org/10.1016/j.wear.2019.01.057.

[21] Qi H.S., Noor K., Day A.J. Interface temperatures in friction braking. Proceedings of the International Conference 'Braking 2002—from the driver to the road' 2002;319–328.

[22] Brake Linings Standards Committee. Brake Lining Quality Test Procedure J661_202110 2021.

[23] Straffelini G, Verma PC, Metinoz I, Ciudin R, Perricone G, Gialanella S. Wear behavior of a low metallic friction material dry sliding against a cast iron disc: Role of the heat-treatment of the disc. Wear 2016;348–349:10–6. https://doi.org/10.1016/j.wear.2015.11.020.

[24] Neis PD, Ferreira NF, Sukumaran J, De Baets P, Ando M, Matozo LT, et al. Characterization of surface morphology and its correlation with friction performance of brake pads. Int J Sustain Constr Des 2016;6:6. https://doi.org/10.21825/scad.v6i1.1136.

[25] Eriksson M, Jacobson S. Tribological surfaces of organic brake pads. Tribol Int 2000;33:817–27. https://doi.org/10.1016/S0301-679X(00)00127-4.

[26] F. Limmer A. Paulus D. Barton P. Brooks A. Neville S. Kosarieh A Comparison of Methods for Characterizing Brake Pad Surfaces. Eurobrake 2020 Conf. Proc 2020.

[27] Österle W, Kloß H, Urban I, Dmitriev AI. Towards a better understanding of brake friction materials. Wear 2007;263:1189–201. https://doi.org/10.1016/j.wear.2006.12.020.

[28] Zoppi A, Lofrumento C, Castellucci EM, Migliorini MG. The Raman spectrum of hematite: Possible indicator for a compositional or firing distinction among Terra Sigillata wares. Ann Chim 2005;95:239–46. https://doi.org/10.1002/adic.200590026.

[29] Fouvry S, Liskiewicz T, Kapsa P, Hannel S, Sauger E. An energy description of wear mechanisms and its applications to oscillating sliding contacts. Wear 2003;255:287–98. https://doi.org/10.1016/S0043-1648(03)00117-0.

[30] Newcomb TP. Temperatures Reached in Disc Brakes. J Mech Eng Sci 1960;2:167–77. 10.1243/JMES_JOUR_1960_002_026_02.

[31] Sarip S, Day AJ, Olley P, Qi HS. Analysis of temperature and pressure distribution in brake disc for regenerative braking. Flex Autom Intell Manuf 2009:8.

[32] Day AJ, Bryant D. Braking of Road Vehicles. Elsevier,; 2022. https://doi.org/10.1016/C2019-0-04185-4.

[33] Newcomb TP, Millner N. Cooling Rates of Brake Drums and Discs. Proc Inst Mech Eng Automob Div 1965;180:191–205. https://doi.org/10.1243/PIME_AUTO_1965_180_019_02.

[34] Jaeger JC. Moving sources of heat and the temperature at sliding contacts. J Proc R Soc N South Wales 1942;75–76:203–24.

[35] Archard JF. The temperature of rubbing surfaces. Wear 1959;2:438–55. https://doi.org/10.1016/0043-1648(59)90159-0.

[36] Smith EH, Arnell RD. A New Approach to the Calculation of Flash Temperatures in Dry, Sliding Contacts. Tribol Lett 2013;52:407–14. https://doi.org/10.1007/s11249-013-0224-9.

[37] Laraqi N, Alilat N, de Maria JMG, Baïri A. Temperature and division of heat in a pin-on-disc frictional device—Exact analytical solution. Wear 2009;266:765–70. https://doi.org/10.1016/j.wear.2008.08.016.

[38] Alilat N, Roseiro L, Ruiz JAL, Guenoun S, Guttiérez F, Laraqi N, et al. Influence of Geometrical and Thermal Parameters on the Thermal Comportment of a Pin-on-Disk System. Proc 7th Int Conf Heat Transf Fluid Mech Thermodyn HEFAT2010 2010:913–7.

[39] Beygelzimer E, Beygelzimer Y. Thermal conductivity of oxide scale and its components in the range from 0C to 1300C: Generalized estimates with account for movability of phase transitions. ArXiv 2021. https://doi.org/10.48550/ARXIV.2110.11632.

[40] Limmer F., Barton D., Brooks P., Gilkeson C., Kosarieh S. Development of a Small-Scale Test Bench for Investigating the Tribology and Emission Behaviour of Novel Brake Friction Couples. EuroBrake 2021 Conf. Proc., 2021.